Available online at www.sciencedirect.com
ScienceDirect
Journal of the European Ceramic Society 26 (2006) 3145–3151
www.elsevier.com/locate/jeurceramsoc

Comparison of nanosized zirconia synthesized by gas and liquid phase methods

Vladimir V. Srdić [a,*], Markus Winterer [b,1]

[a] *Faculty of Technology, University of Novi Sad, Novi Sad, Serbia and Montenegro*
[b] *Institute of Materials Science, Darmstadt University of Technology, Darmstadt, Germany*

Received 2 April 2005; received in revised form 17 October 2005; accepted 29 October 2005
Available online 12 January 2006

Abstract

Pure zirconia nanopowders prepared by gas phase (chemical vapor synthesis and inert gas condensation) and liquid phase methods (sol–gel synthesis) exhibit similar primary particle size and surface area. However, the characteristics regarding compaction and sinterability are quite different.

Keywords: Powders-gas phase reaction; Powders-chemical preparation; ZrO_2

1. Introduction

The term nanopowder is commonly used to describe a ceramic powder with superior sinterability where 'nano' usually relates only to crystallite or primary particle sizes in the nanometer regime. However, it is well known[1] that, for example, the presence of agglomerates, i.e. the microstructure of the powder particles and their size play an important role in the densification process and may impede preparation of dense ceramic bodies with grain size smaller than 100 nm. Thus, it is important to clearly distinguish between nanopowders prepared by different synthesis techniques. Synthesis of high-purity, ultra-fine and agglomerate free zirconia powders with narrow size distributions is the first and perhaps most important step in producing nanocrystalline zirconia ceramics with desirable microstructure and properties. Very popular methods for the synthesis of zirconia nanopowders are *liquid phase techniques* (usually called *wet-chemical synthesis*), such as gel precipitation, using either an alkoxide or the chloride method.[1–6] These processes are based on complex sol–gel chemistry, require little capital investment and enable the production of relatively large quantities of high purity zirconia powders of very fine crystallite size. On the other hand, various *gas phase processes* (inert gas condensation,[7,8] laser ablation,[9,10] microwave plasma synthesis,[11] chemical vapor synthesis,[12–15] etc.) have been widely used for the production of loosely agglomerated or nonagglomerated nanocrystalline zirconia powders with controlled size, size distribution, and a low degree of impurities.

This paper compares three different zirconia nanopowders regarding their compaction and sinterability. Two have been synthesized by gas phase techniques: inert gas condensation (IGC) and chemical vapor synthesis (CVS), and one by the most common liquid phase method, called wet-chemical synthesis by controlled alkoxide hydrolysis (WCS).

2. Experimental procedures

2.1. Powder synthesis

2.1.1. Chemical vapor synthesis

The CVS nanocrystalline ZrO_2 powder was synthesized in a hot wall reactor (for details see ref.[16]). The liquid zirconium-tertiary-butoxide precursor ($Zr(O^tC_4H_9)_4$, Inorgtech, England) is delivered to the reaction zone by a controlled flow of helium gas through a bubbler held at 80 °C. An additional flow of oxygen entering directly into the reacting zone assures complete oxidation of the product. During the short residence time of

* Corresponding author. Tel.: +381 21 450 288; fax: +381 21 450 413.
E-mail addresses: srdicvv@uns.ns.ac.yu (V.V. Srdić), markus.winterer@uni-duisburg.de (M. Winterer).
[1] Present address: Nanoparticle Process Technology, University of Duisburg-Essen, Duisburg, Germany. Tel.: +49 203 379 4446; fax: +49 203 379 4453.

0955-2219/$ – see front matter © 2005 Elsevier Ltd. All rights reserved.
doi:10.1016/j.jeurceramsoc.2005.10.006

about 10 ms in the hot zone, at 1000 °C and 1000 Pa, precursor molecules are decomposed forming small oxide nanoparticles according to:

$$Zr(O^tC_4H_9)_{4[vapor]} + O_2 \overset{1000\,^\circ C,\ 1000\,Pa}{\longrightarrow} ZrO_{2[nano\text{-}powder]} + \text{by-products.} \quad (1)$$

The zirconia nanoparticles are then collected from the aerosol on the wall of the metal tube due to the thermophoretic force produced by the temperature gradient between the heated quartz lamp (positioned inside the tube) and the water-cooled wall of the metal tube. The collected material is similar to an aerogel (see, e.g. ref.[17]).

2.1.2. Inert gas condensation

The IGC zirconia nanopowder was cluster-assembled in an ultra-high vacuum chamber.[8] Zirconium suboxide granules (ZrO, Balzers, Liechtenstein) are evaporated in a low pressure (1 Pa) helium atmosphere. Particles are formed above the evaporation source by homogeneous nucleation and transported by a convective gas flow to a cold plate cooled by liquid nitrogen. The nanoparticles are extracted from the gas flow by thermophoretic forces and deposited on the surface of the cold plate. The collected zirconium-suboxide nanoparticles are finally annealed in an oxygen atmosphere at 300 °C to convert them into fully stoichiometric ZrO_2. The overall process can be schematically represented by two equations:

$$ZrO_{[coarse\text{-}powder]} \overset{1800\,^\circ C,\ 1\,Pa}{\longrightarrow} ZrO_{[nano\text{-}powder]} \quad (2)$$

$$ZrO_{2[nano\text{-}powder]} + \tfrac{1}{2}O_2 \overset{350\,^\circ C}{\longrightarrow} ZrO_{[nano\text{-}powder]} \quad (3)$$

2.1.3. Wet-chemical synthesis

The WCS zirconia nanopowder was synthesized by hydrolysis of zirconium-*n*-propoxide (e.g. ref.[18]). Zirconium-*n*-propoxide ($Zr(O^nC_3H_7)_4$, Fluka, Switzerland) is dissolved in anhydrous ethanol and hydrolyzed with distilled water under acidic condition (pH ~ 1) at room temperature (alkoxide, water and hydrochloric acid molar ratio was 1:2:0.5). An aqueous sol is obtained by continuous evaporation and replacement of ethanol with distilled water without changing concentration and pH. The hydroxides are then precipitated by slowly adding this aqueous sol to a well-stirred ammonium hydroxide solution (pH > 11). The precipitated powder is washed with distilled water until the effluent is free of Cl^- (determined qualitatively using a silver-nitrate solution) and than three times with absolute ethanol to remove free water and replace the particle surface hydroxyl with ethoxy groups. After washing, the gel nanopowder is filtered, dried at 120 °C for 1 day, dry milled (as-synthesized WCS powder) and calcined at 500 °C for 1 h (calcined WCS powder). The overall process can be expressed as:

$$Zr(O^nC_3H_7)_{4[ethanol\text{-}solution]} + 4H_2O \overset{25\,^\circ C}{\longrightarrow} Zr(OH)_{4[nano\text{-}powder]} + 4C_3H_7OH \quad (4)$$

$$Zr(OH)_{4[nano\text{-}powder]} \overset{500\,^\circ C}{\longrightarrow} ZrO_{2[nano\text{-}powder]} + 2H_2O \quad (5)$$

2.2. Compaction and sintering

Green pellets are prepared with as-synthesized CVS, as-synthesized (annealed at 300 °C) IGC and calcined (at 500 °C) WCS nanopowders. Nanopowders are uniaxially pressed in a hard metal die with a diameter of 8 mm at room temperature and 500 MPa. The pressed pellets are heated with a heating rate of 5 °C/min, held at 350 °C for 1 h, then at 500 °C for 1 h and finally pressureless sintered in air or in vacuum (0.5 Pa) at different temperatures up to 1100 °C. The oxygen loss during vacuum sintering has been recovered by cooling down in an oxygen flow of about 200 cm^3/min at normal pressure.

2.3. Characterization

The specific surface area of the CVS, IGC and WCS zirconia nanopowders was measured by nitrogen adsorption analyzed according to the BET method using a Quantachrom Autosorb-3B instrument. The particle size was calculated from the specific surface area assuming spherically shaped, monodisperse particles, by $d_{BET} = 6/(\rho S_v)$, where ρ is the density and S_v the specific surface area of the sample. The X-ray diffraction measurements were performed with a Siemens D5000 instrument for the analysis of the zirconia phases and crystallite size. The phase ratio was determined using the integrated intensity of the tetragonal (1 1 1) and monoclinic (1 1 1) and (1 1 $\bar{1}$) Bragg reflections. The crystallite size of the zirconia powders was estimated from the full width at half maximum using the Scherrer equation ($d = 0.9\lambda/(\beta \cos\theta)$), where λ is the wavelength of the X-rays, θ the scattering angle of the Bragg reflections and β the full width at half maximum corrected for instrumental broadening). Additionally, the crystallite size, size distribution, structure and morphology of the zirconia powders were investigated from transmission electron microscopy (TEM) images obtained with a Philips CM20 Ultra Twin microscope operating at 200 kV.

The density of the pressed and sintered pellets was measured from geometry and mass of the sample. The pore size distribution of these samples was determined by low-temperature nitrogen adsorption from the adsorption and desorption isotherms according to the BJH theory (assuming cylindrical pore geometry).[19] The microstructure of fresh fractured sample surfaces was examined using a high resolution scanning electron microscope (HRSEM Philips XS 30) operating at 20 kV.

3. Results

Microstructural characteristics of the as-synthesized CVS and IGC zirconia powders are quite similar (Table 1). Both consist of flaky aerogels of very low density, which were formed by collecting primary nanoparticles from the gas phase. Both powders are crystalline, consisting of a mixture of tetragonal and monoclinic zirconia phases (Fig. 1a), with an average crystallite size estimated from XRD of about 5 nm and relatively high specific surface areas of about 220 m^2/g corresponding to a particle size of 4.6 nm (Table 1). High-resolution TEM micrographs of the CVS and IGC zirconia nanopowders are shown in Fig. 2. The CVS powder is very fine, well crystallized without defects,

Table 1
Characteristics of as-synthesized and calcined zirconia nanopowders

	CVS		IGC		WCS	
	Synthesized	Calcined[a]	Synthesized	Calcined[a]	Synthesized	Calcined[a]
Specific surface area (m^2/g)	224	103	222	98	294	129
Particle size from BET (nm)	4.6	10.0	4.6	10.5	3.5	8.0
Crystallite size of t-ZrO_2 (nm)	4.6	7.5	4.1	8.8	–	7.3
Crystallite size of m-ZrO_2 (nm)	6.1	8.0	5.6	8.8	–	5.8
Volume fraction of t-ZrO_2 (%)	77	42	71	54	Amorphous	90
Particle size from TEM (nm)	5.7	–	7.2	–	–	–
Mass loss (heating up to 1000 °C) (%)	10.2		–		24.1	

[a] Powders were calcined in air at 500 °C for 1 h.

nonagglomerated and consists mostly of facetted crystallites exhibiting low energy surfaces. The particle size distribution of the CVS powder, obtained from the TEM micrographs,[16] is well-fitted by a log-normal distribution function (Fig. 3) giving a geometric mean crystallite size of 5.7 nm and a small geometric standard deviation of 1.24. The average particle size of the IGC powder, measured by HRTEM, is 7.2 nm, with geometrical standard deviation of 1.3 (Fig. 3, Table 1). It is obvious (Fig. 3) that both the standard and even the best IGC powder[8] have broader size distributions in comparison with the CVS zirconia nanopowder.

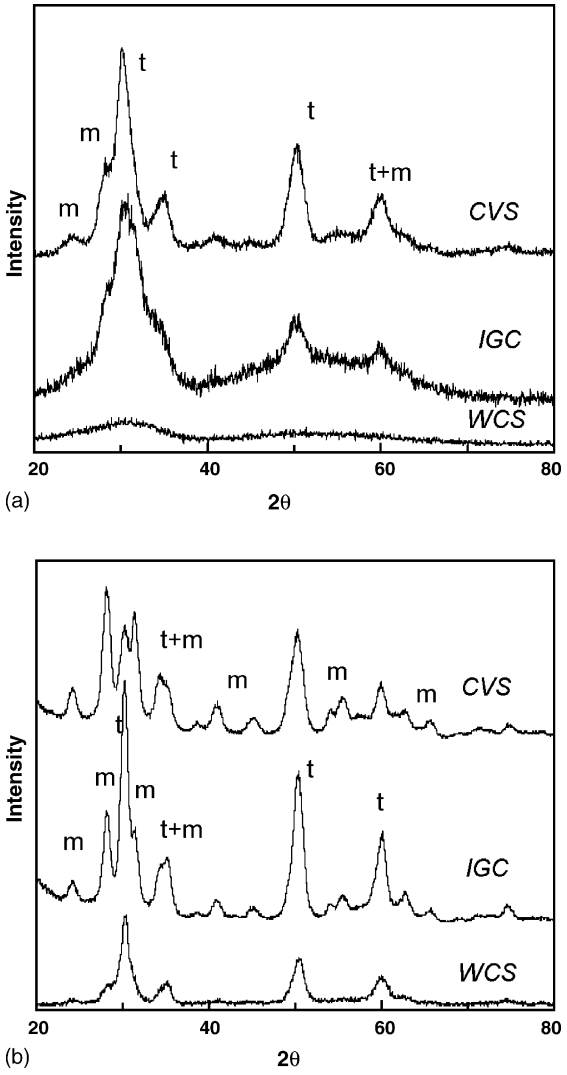

Fig. 1. X-ray diffraction patterns of CVS, IGC and WCS samples: (a) as-synthesized powders and (b) powders calcined at 500 °C (m: monoclinic zirconia, t: tetragonal zirconia).

In contrast, the *as-synthesized* WCS zirconia powder is amorphous (Fig. 1a) and has a somewhat higher specific surface area, of 294 m^2/g, than both CVS and IGC powders synthesized from vapor phase (Table 1). The mass loss of 24.1% occurring on heating up to 1000 °C is very close to 22.4% which corresponds to a complete conversion of the hydroxide $Zr(OH)_4$ into the dioxide ZrO_2 as described by Eq. (5), indicating the character of the as-synthesized powder. The as-synthesized zirconia powder crystallizes at 460 °C (confirmed by DTA) and the powder calcined at 500 °C for 1 h consists of tetragonal zirconia with a small amount of the monoclinic phase (Fig. 1b). The average crystallite size can be estimated by XRD to about 7 nm which is somewhat smaller than the average particle size calculated by BET (Table 1), indicating the formation of hard agglomerates in the calcined WCS nanopowder. High crystallinity of the calcined WCS particles and their agglomerated state is observed by HRTEM, Fig. 2c. It seems that the stability of the tetragonal crystallites during calcination is higher in the WCS nanopowder (Fig. 1b) in comparison to powders produced by IGC or CVS.

Low-temperature nitrogen adsorption measurements, presented in Fig. 4, show considerably differences between the vapor synthesized (IGC and CVS) and the WCS zirconia powders. The adsorption/desorption hysteresis of the as-synthesized IGC and CVS powders is of type II (similar to aerogels) indicating a low degree of hard agglomeration (Fig. 4a and b), whereas presence of hard agglomeration is confirmed with the shape of the adsorption/desorption hysteresis loop of the as-synthesized WCS powder (Fig. 4c). The characteristic type IV shape of the hysteresis loop originates in the mesoporosity of the as-synthesized WCS particles (agglomerates) and the ink-bottle shape of intraparticle pores. The mesoporous nature of the as-synthesized WCS powder can be easily detected in the pore size distribution curve, presented in Fig. 5. The nitrogen adsorption results show that during calcination the specific surface area decreases considerably from 294 to 129 m^2/g and pores smaller than 2 nm disappear, indicating neck formation between primary nanoparticles and most probably the formation of hard agglomerates. These are the reasons why the pore size distribution curves of the calcined WCS nanopowder and the pressed

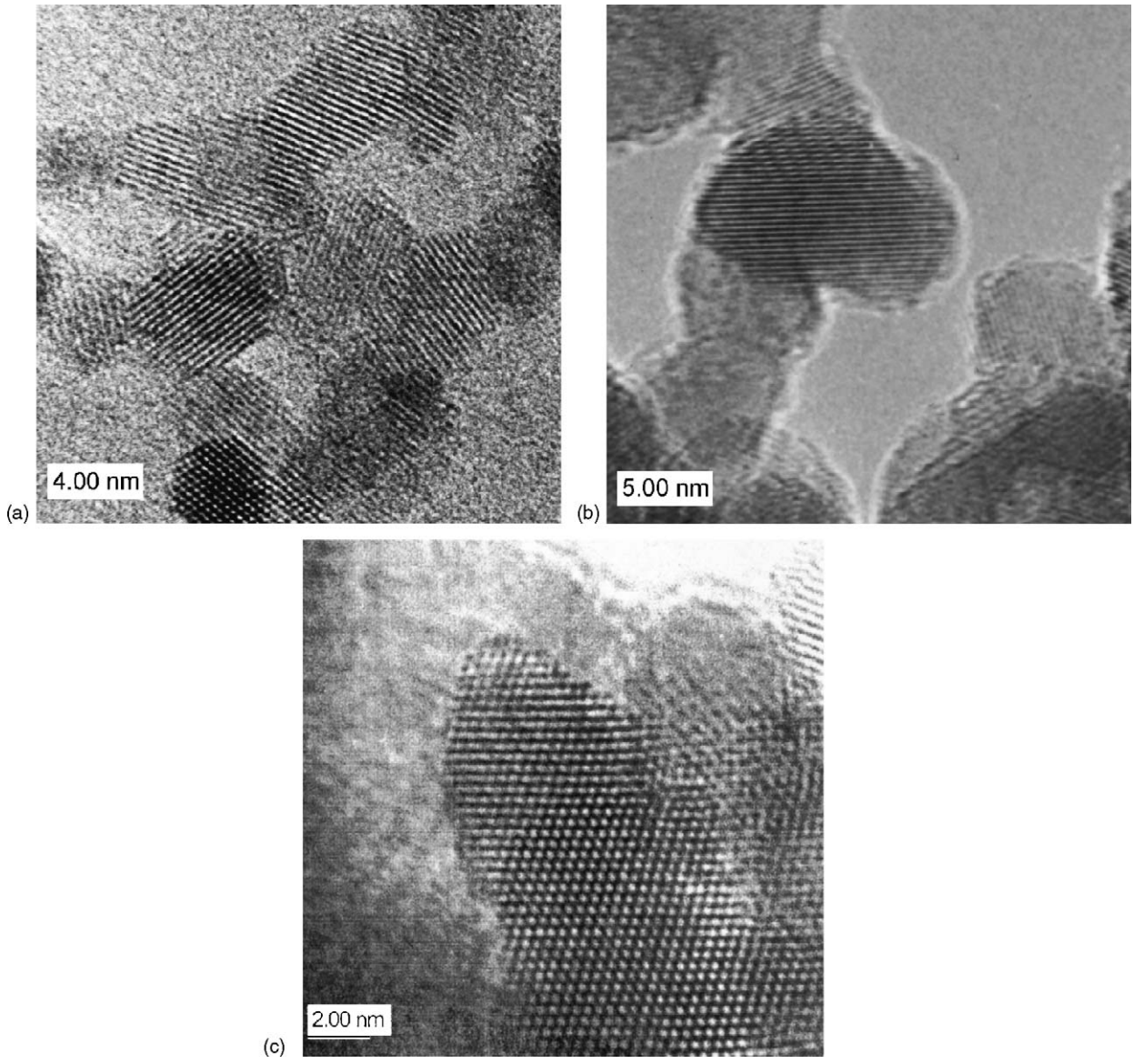

Fig. 2. HRTEM micrographs of: (a) as-synthesized CVS, (b) as-synthesized IGC and (c) calcined WCS zirconia nanopowders.

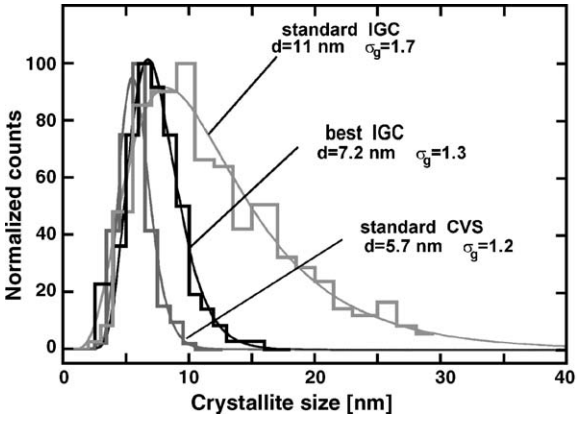

Fig. 3. Crystallite size distribution of as-synthesized standard CVS, standard IGC and best IGC zirconia nanopowders.

WCS pellet are very similar (Fig. 5), i.e. the mesopores smaller that 10 nm in the calcined WCS zirconia nanopowder do not change even after uniaxial pressing at 500 MPa. This observation is in contrast to observation for the CVS powder and pressed pellet (Fig. 6) and, similarly, to zirconia produced by IGC[20] where the broad pore size distribution observed for the as-synthesized powders collapses upon compaction and sintering as the original aerogel network is destroyed.

Relative densities of the as-synthesized CVS and calcined WCS powder compacts as a function of the logarithm of the applied pressure are presented in Fig. 7. The compaction behavior of the CVS nanopowder can be described by a simple logarithmic correlation indicating a nonagglomerated state. In contrast, the WCS zirconia powder has a curve with two logarithmic dependencies with the point of intersection at a pressure of about 60 MPa. This is a clear indication of the agglomerated nature of the WCS zirconia powder.[1] The agglomeration

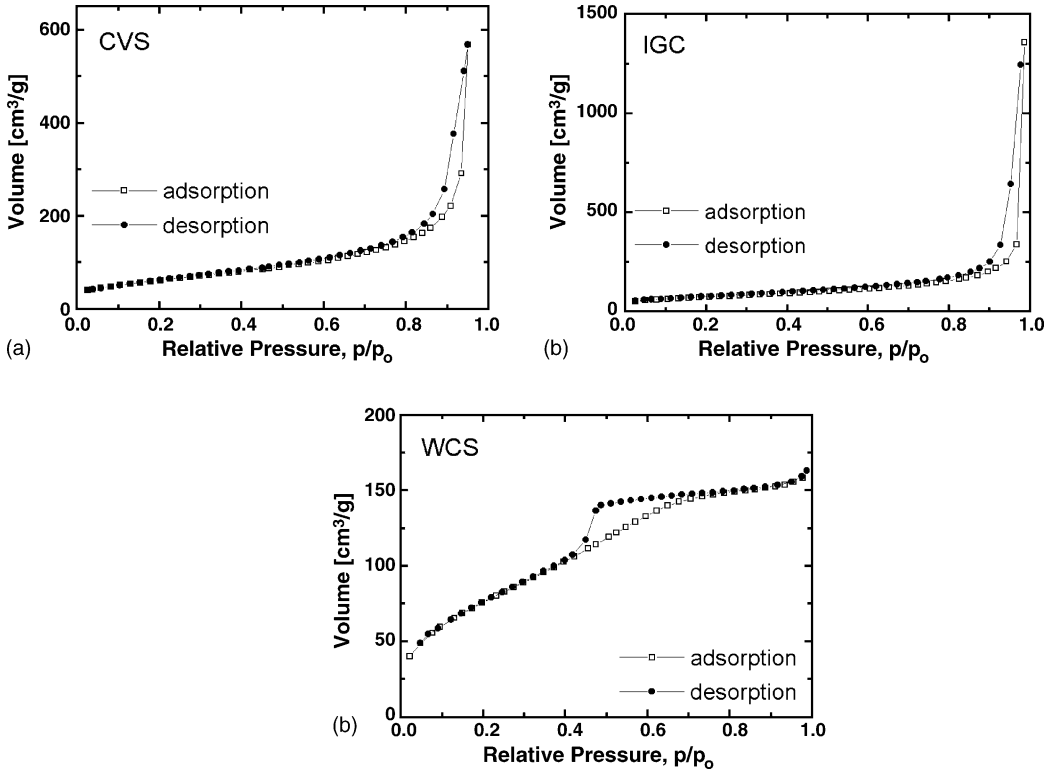

Fig. 4. Adsorption/desorption hysteresis obtained by low-temperature nitrogen adsorption measurement for as-synthesized: (a) CVS, (b) IGC and WCS zirconia nanopowders.

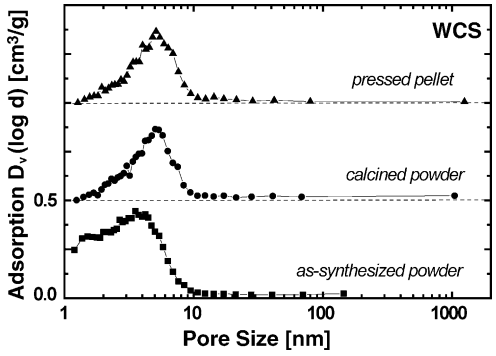

Fig. 5. Pore size distribution from the adsorption branch of nitrogen sorption isotherms of WCS samples: as-synthesized powder, calcined powders, and pressed pellet.

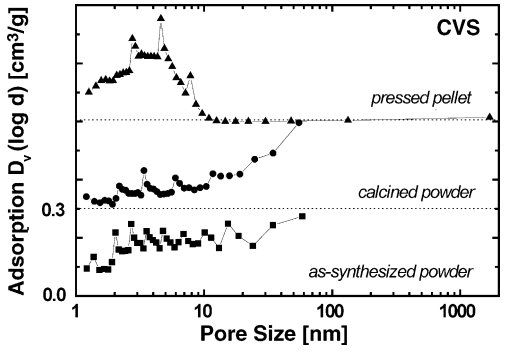

Fig. 6. Pore size distribution from the adsorption branch of nitrogen sorption isotherms of CVS samples: as-synthesized powder, calcined powders, and pressed pellet.

of the calcined WCS powder is the main reason for the coarser microstructure of the WCS compared to the CVS pressed pellet (Fig. 8).

It is well known that not only compaction but also sinterability strongly depends on powder characteristics.[21,22] Thus, the sintering results, presented in Fig. 9, show that the agglomerated WCS zirconia nanopowder has poor sinterability in comparison to the vapor synthesized powders. After vacuum sintering the WCS zirconia reached a density of about 92%TD at 1000 °C (Fig. 9). On the other hand, densities higher that 95%TD could be reached in the IGC and CVS zirconia after vacuum sintering already at 850 °C (Fig. 9). Theoretically dense samples can be obtained by vacuum sintering at 1000 °C for IGC zirconia,[23] whereas at 950 °C for CVS zirconia.[16] In addition, the fully

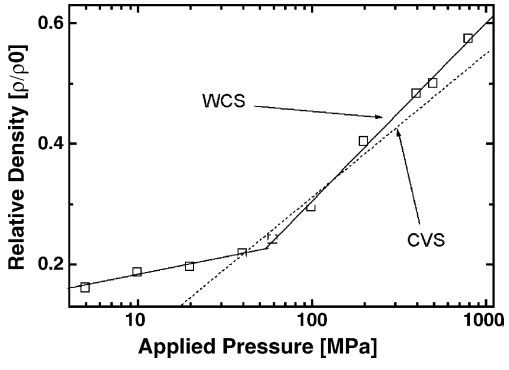

Fig. 7. Relative density of green CVS and WCS compacts versus applied pressure.

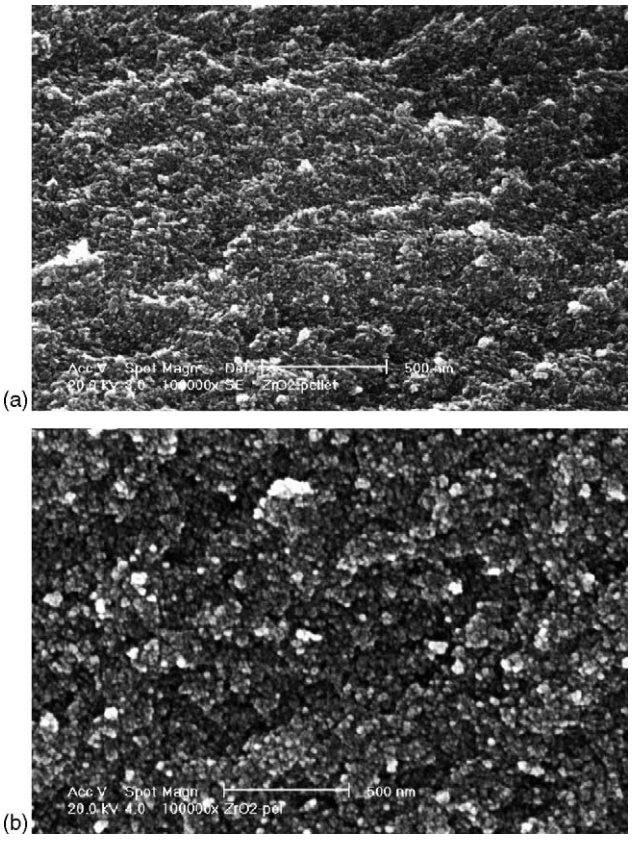

Fig. 8. Microstructure of uniaxially pressed pellets prepared with: (a) CVS and (b) WCS nanopowders.

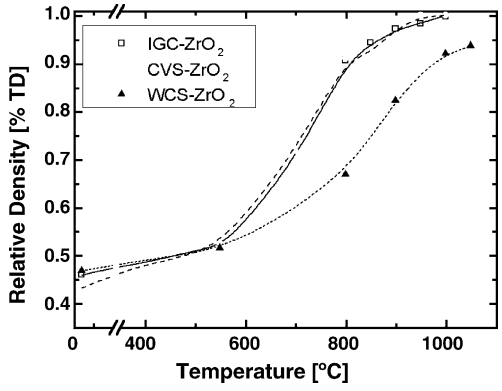

Fig. 9. Relative density change with sintering temperature for CVS, IGC and WCS pellets sintered in air and vacuum (CVS and WCS pellets are sintered in air for 3 h, whereas IGC pellets are sintered in air for 2 h).

dense CVS zirconia pellet with a grain size of about 60 nm and a thickness of 0.32 mm is transparent[16] whereas the WCS pellets are not transparent. However, IGC zirconia, while transparent in the as-compacted state, loses transparency at sintering temperatures of ~500–600 °C.[24]

4. Conclusions

Nanocrystalline pure zirconia powders of mainly tetragonal phase, an average crystallite size of 5 nm and high surface area of about 220 m^2/g are synthesized by gas phase methods (chemical vapor synthesis and inert gas condensation). Zirconia powders with similar primary particle size and surface area, but with an amorphous structure, are synthesized by a liquid phase method (sol–gel synthesis). The main difference between nanopowders prepared from the gas phase and liquid phase methods, determining compaction and sintering behavior, is the microstructure of the powder particles, particularly the state of agglomeration.

Ultrafine zirconia powders produced by chemical vapor synthesis show the best sinterability of the investigated materials. Compaction, sinterability and final microstructure are largely influenced by the microstructural characteristics of the as synthesized powders which depend highly on the method of synthesis and process parameters.

Acknowledgements

The authors gratefully acknowlegde the support by the Alexander von Humboldt foundation and the German Science Foundation. We also like to thank Dr. Robert Nitsche for discussions and Dr. Gerhard Miehe for preparation of the HRTEM images.

References

1. Groot-Zevert, W. F. M., Winnubst, A. J. A., Theunissen, G. S. A. M. and Burggraaf, A. J., Powder preparation and compaction behavior of fine-grained Y-TZP. *J. Mater. Sci.*, 1990, **25**, 3449–3455.
2. van de Graaf, M. A. C. G. and Burggraaf, A. J., Wet-chemical preparation of zirconia powders: their microstructure and behavior. In *Advance in Ceramics, Science and Technology of Zirconia II*, ed. N. Claussen *et al.* American Ceramics Society, Columbus, OH, 1983, pp. 744–765.
3. Benedetti, A., Fagherazzi, G., Pinna, F. and Polizzi, S., Structural properties of ultra-fine zirconia powders obtained by precipitation methods. *J. Mater. Sci.*, 1990, **25**, 1473–1478.
4. Duricic, B., Kolar, D. and Komac, M., Synthesis and characterizations of zirconia fine powders from organic zirconium complexes. *J. Mater. Sci.*, 1990, **25**, 1132–1136.
5. Sagel-Ransijn, C. D., Winnubst, A. J. A., Burggraaf, A. J. and Verweij, H., The influence of crystallization and washing medium on the characteristics of nanocrystalline Y-TZP. *J. Eur. Ceram. Soc.*, 1996, **16**, 759–766.
6. Wu, N. L. and Wu, T. F., Enhanced phase stability for tetragonal zirconia in precipitation synthesis. *J. Am. Ceram. Soc.*, 2000, **83**(2), 3225–3227.
7. Hahn, H., Eastman, J. A. and Siegel, R. W., Processing of nanophase ceramics. In *Ceramic Transactions Vol. 1b, Ceramic Powder Science II*, ed. G. L. Messing, E. R. Fuller and H. Hausner. America Ceramic Society, Westerville, OH, 1998, pp. 1115–1118.
8. Nitsche, R., Rodewald, M., Skandan, G., Fuess, H. and Hahn, H., HRTEM study of nanocrystalline zirconia powders. *Nanostruct. Mater.*, 1996, **7**(5), 535–546.
9. Lee, H. Y., Riehemann, W. and Mordike, B. L., Sintering of nanocrystalline ZrO_2 and zirconia toughened alumina (ZTA). *J. Eur. Ceram. Soc.*, 1992, **10**, 245–253.
10. Ferkel, H., Naser, J. and Riehemann, W., Laser-induced solid solution of the binary nanoparticle system Al_2O_3–ZrO_2. *Nanostruct. Mater.*, 1997, **8**(4), 457–464.
11. Vollath, D. and Sickafus, K. E., Synthesis of nanosized ceramic oxide powders by microwave plasma reactions. *Nanostruct. Mater.*, 1992, **1**, 427–437.
12. Mazdiyasni, K. S., Lynch, C. T. and Smith, J. S., Preparation of ultra-high-purity submicron refractory oxides. *J. Am. Ceram. Soc.*, 1965, **48**(7), 372–375.

13. Chang, W., Skandan, G., Danforth, S. C., Kear, B. H. and Hahn, H., Chemical vapor processing and application for nanostructured ceramic powders and whiskers. *Nanostruct. Mater.*, 1994, **4**(5), 507–520.
14. Srdic, V. V., Winterer, M. and Hahn, H., Different zirconia-alumina nanoparticles by modifications of chemical vapor synthesis. *Nanostruct. Mater.*, 1999, **12**, 95–100.
15. Benfer, S. and Knozinger, E., Structure morphology and surface properties of nanostructured ZrO_2 particles. *J. Mater. Chem.*, 1999, **9**, 1203–1209.
16. Srdic, V. V., Winterer, M. and Hahn, H., Sintering behavior of nanocrystalline zirconia prepared by chemical vapor synthesis. *J. Am. Ceram. Soc.*, 2000, **83**(4), 729–736.
17. Winterer, M., *Nanocrystalline Ceramics – Synthesis and Structure*. Springer, Heidelberg, 2002.
18. Srdic, V. V. and Radonjic, L., Synthesis and sintering behavior of nanocrystalline ZrO_2-3 mol% Y_2O_3 powders. *Key Eng. Mater.*, 1997, **132–136**, 45–48.
19. Barrett, E. P., Joyner, L. G. and Helenda, P. P., The determination of pore volume and area distributions in porous substrates, I Computations from nitrogen isotherms. *J. Am. Ceram. Soc.*, 1951, **73**, 373–380.
20. Allen, A. J., Krueger, S., Skandan, G., Long, G. G., Hahn, H., Kerch, H. M. *et al.*, Microstructural evolution during sintering of nanostructured ceramic oxides. *J. Am. Ceram. Soc.*, 1996, **79**, 1201–12012.
21. Rhodes, W. H., Agglomerate and particle size effects on sintering yttria-stabilized zirconia. *J. Am. Ceram. Soc.*, 1981, **64**(1), 19–22.
22. Mayo, M. J., Hague, D. C. and Chen, D. J., Processing nanocristalline ceramics for applications in superplasticity. *Mater. Sci. Eng.*, 1993, **A166**, 145–159.
23. Skandan, G., Hahn, H., Roddy, M. and Cannon, W. R., Ultrafine-grained dense monoclinic and tetragonal zirconia. *J. Am. Ceram. Soc.*, 1994, **77**(7), 1706–1710.
24. Skandan G. and Hahn, H., unpublished results.